JOURNAL OF MOLECULAR SPECTROSCOPY 100, 303–315 (1983)

Laser Magnetic Resonance of the O_2 Molecule at 699 μm[1]

MASATAKA MIZUSHIMA

Department of Physics, University of Colorado, Boulder, Colorado 80309

K. M. EVENSON, J. A. MUCHA, AND D. A. JENNINGS

Time and Frequency Division, National Bureau of Standards, Boulder, Colorado 80303

AND

J. M. BROWN

Department of Chemistry, The University, Southampton, S09 5NH, England

A new highly sensitive far infrared optically pumped laser magnetic resonance (LMR) spectrometer has facilitated the observation of 21 transitions in O_2 at 699 μm (428.6285 GHz). All of these transitions involve $N = 3 \leftarrow 1$ of the oxygen molecule in its electronic ground state, $X^3\Sigma_g^-$. Of these 21 lines, 10 are due to the $^{16}O_2$, $v = 0$; 5 are due to the $^{16}O_2$, $v = 1$; 5 are due to the $^{16}O^{18}O$, $v = 0$; and 1 set of 6 hyperfine components is due to the $^{16}O^{17}O$, $v = 0$. From the intensity of the observed lines the sensitivity limit of this LMR spectrometer is found to be about 10^{-9} cm^{-1} at this frequency with a 1-sec time constant.

INTRODUCTION

The first gas phase laser magnetic resonance (LMR) spectrum was observed by Evenson *et al.* (*1*) on the $N = 5 \leftarrow 3$ transition of the oxygen molecule, $^{16}O_2$ ($X^3\Sigma_g^-$, $v = 0$) using the 337-μm HCN laser line. The analysis was later refined by Mizushima *et al.* (*2*). Since then, four other rotational transitions of the $^{16}O_2$ molecule have been observed using the LMR technique, namely, the $N = 15 \leftarrow 13$ and $23 \leftarrow 21$ transitions using H_2O laser lines (*3*), and $N = 17 \leftarrow 15$ and $21 \leftarrow 19$ transitions using D_2O laser lines (*4*). All of these were observed in LMR spectrometers using electrical discharges for excitation. A new LMR spectrometer with optically pumped excitation has permitted the observation of some extremely weak transitions in oxygen at a wavelength of 699 μm (428.6285 GHz). The $N = 3 \leftarrow 1$ transitions of $^{16}O_2$ and other isotopic species of this molecule are assigned in this paper. The $N = 3 \leftarrow 1$ transitions of the $^{16}O_2$ molecule have been observed by McKnight and Gordy (*5*) and Steinbach and Gordy (*6*) in submillimeter absorption spectroscopy. They reported an energy separation between the ($N = J = 1$) and ($N = J = 3$) states of 430.984697(60) GHz, which is confirmed by our present result. In addition to these transitions due to the $^{16}O_2$ molecule in the vibrational ground state ($v = 0$), we

[1] Supported in part by NASA Grant W-15,047.

0022-2852/83 $3.00

observed transitions due to its isotopic species: $^{16}O^{17}O$ and $^{16}O^{18}O$ both in their natural abundances, 0.074 and 0.408%, respectively, and transitions due to $^{16}O_2$ in the $v = 1$ state. Amano and Hirota (*7*) observed the 60-GHz transitions for all of these except those of $^{16}O^{17}O$; Endo and Mizushima (*8*) observed 60- and 119-GHz transitions of $^{16}O_2$, in both $v = 0$ and 1 states; Steinbach and Gordy (*9*) observed microwave and submillimeter transitions of $^{16}O^{18}O$, and Cazzoli *et al.* (*10*) observed microwave transitions of $^{16}O^{17}O$ and $^{17}O^{18}O$.

EXPERIMENTAL DETAILS

A new FIR LMR spectrometer has been constructed in our NBS Boulder laboratory which is about five times more sensitive, allows more lines to lase, and is significantly easier to operate. The new spectrometer is shown in Fig. 1. A 38-cm electromagnet with ring-shimmed hyperco pole caps produces a 7.5-cm homogeneous field region of five times greater length along the laser axis than that of our previous spectrometer; thus, it is about five times more sensitive. The new FIR cavity is 25 cm shorter and oscillates to wavelengths up to 1000 μm. Better overlap between pump and FIR laser yields a lower threshold of oscillation and, consequently, a larger number of FIR lines. The improved overlap was accomplished with a nearly confocal mirror geometry, the insertion of the CO_2 pump at the beam waist, and the use of a cylindrical gold-coated pyrex tube as the CO_2 reflector. This cylindrical tube was found to double the output power in a FIR laser compared with the use of flat side mirrors. A 10-cm i.d. gold-coated copper tube is used as the first cylindrical CO_2 beam focuser and is then followed by a series of consecutive refoci from the walls of the pyrex tube. Quartz is used for the spacers in the spectrometer to provide better thermal stability. For ease

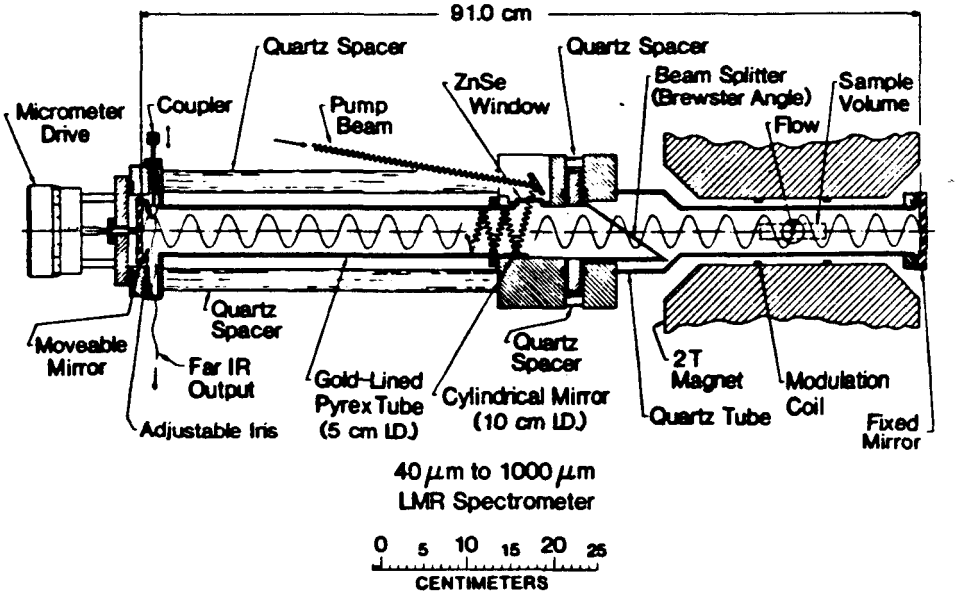

FIG. 1. The new LMR spectrometer.

of operation, the micrometer, coupler, detector, CO_2 laser grating, and gas handling system are all accessible from one side of the magnet. The beam splitter is rotatable about the laser axis so that the polarization can be changed. The magnet controlled by a rotating coil is calibrated periodically with an NMR gaussmeter. The overall fractional uncertainty above 0.1 T is 10^{-4}; below 0.1 T the absolute uncertainty is 10^{-5} T.

ANALYSIS

$^{16}O_2$ ($X^3\Sigma_g^-$, $v = 0$)

The theory of the rotational energy levels of the oxygen molecule in its electronic ground state, $X^3\Sigma_g^-$ is well established (*11, 12*). It is found that all existing microwave (*7, 8, 12*), and submillimeter (*5, 6*) free field data of $^{16}O_2$ ($X^3\Sigma_g^-$, $v = 0$) can be reproduced by taking the set of molecular parameters (*8*) shown in the first column of Table I.

The EPR spectrum in the microwave region was observed by Bauers *et al.* (*13*) who obtained value for the g factors of

$$g_\perp = 2.004838(30),\ g_\parallel = 2.002025(20),$$

$$g_n = 0.000126(12). \tag{1}$$

We used these g factors and the molecular parameters in Table I to construct a 15×15 Hamiltonian matrix, including $N = 1$, 3, 5, 7, and 9 states for a given magnetic quantum number M and magnetic field B. The matrix was directly diagonalized to obtain eigenvalues and eigenvectors. The values of the resonance fields shown in Table II(1) are obtained by comparing the differences between the lower and upper eigenvalues (corresponding to $N = 1$ and $N = 3$ states) with the laser frequency 428.6285 GHz. The resettability of the laser line gives the uncertainty of this value, 0.3 MHz.

TABLE I

Values of the Molecular Parameters Used in the Calculation ($X^3\Sigma_g^-$ state)

	$^{16}O_2$ v=0	$^{16}O^{17}O$ v=0	$^{16}O^{18}O$ v=0	$^{16}O_2$ v=1
B	43.100430	41.8306	40.707408	42.626398
D	1.436×10^{-4}	1.37×10^{-4}	1.29×10^{-4}	1.489×10^{-4}
λ	59.5013489	59.50009	59.499097	59.646079
λ_D	5.8305×10^{-5}	5.75×10^{-5}	5.312×10^{-5}	6.3257×10^{-5}
λ_{DD}	3.39×10^{-10}			1.51×10^{-10}
γ	-0.2525875	-0.245114	-0.238488	-0.253193
γ_D	-2.4522×10^{-7}	-2.4×10^{-7}	-6.19×10^{-7}	-2.5241×10^{-7}

All values are in GHz

TABLE II

Observed and Calculated Resonance Field, Assignment, Calculated Relative Slope, SQDP, and Peak Intensity of LMR of Oxygen Using the CH_3OH Laser Line (428.6285 GHz)

(1) $^{16}O_2$ v=0

(1a) ΔM=0 transitions.

$B_{obs.}$(Tesla)			0.08666	0.1771	0.2417
$B_{calc.}$(T)	0.01309	0.0261	0.08662	0.17716	0.24175
N=3 (J,M) levels	4,2	4,1	2,-2	2,-1	3,1
N=1 (J,M)	2,2	2,1	2,-2	2,-1	1,1
Relative Slope (T/THz)	-75.	-148.	23.	49.	-127.
SQDP*	3×10^{-7}	2.4×10^{-6}	0.202	0.0461	1.44×10^{-5}
Peak Intensity (cm^{-1})**	3×10^{-11}	2.2×10^{-10}	1.89×10^{-5}	4.3×10^{-6}	1.4×10^{-9}

(1b) ΔM=±1 transitions

$B_{obs.}$(T)					0.10935	0.12451		0.2972***	0.3034	0.31677	0.43451	0.6312
$B_{calc.}$(T)	0.00861	0.01283	0.02507	0.02724	0.10932	0.12445	0.19283	0.29495	0.30336	0.31691	0.43471	0.63177
N=3 (J,M) level	4,1	4,0	4,-1	4,3	2,-1	2,-2	3,0	3,2	2,-2	2,0	4,-1	4,2
N=1 (J,M)	2,2	2,1	2,0	2,2	2,-2	2,-1	1,1	1,1	2,-1	2,-1	2,0	2,1
Relative Slope (T/THz)	-49.	-73.	-143.	-155.	29.	42.	-96.	-149.	-1257.	96.	120.	-1210.
SQDP*	1.5×10^{-8}	1×10^{-7}	2×10^{-7}	1.5×10^{-6}	0.051	0.0105	0.5×10^{-6}	0.39×10^{-4}	0.8×10^{-3}	0.073	0.064	2.4×10^{-3}
Peak Intensity (cm^{-1})**	1.4×10^{-12}	9.0×10^{-11}	2×10^{-11}	1.4×10^{-10}	4.8×10^{-6}	1.0×10^{-6}	4.1×10^{-11}	3.7×10^{-9}	7.4×10^{-8}	6.9×10^{-6}	6.0×10^{-6}	2.3×10^{-7}

*SQDP=(matrix element of magnetic moment/Bohr Magneton)^2.

** Peak intensity is calculated assuming Lorentzian line shape with Δ=11.3 kHz/Pa.

***This line is seen on the shoulder of the stronger and broader line at 0.3034 Tesla.

(2) $^{16}O^{17}O$, v=0

(2a) ΔM=0 transitions

$B_{obs.}$ (T)	0.3711***				
$B_{calc.}$(T)	0.37089	0.6211	0.7435	1.0102	1.8338
N=3 (J,M) level	4,-2	3,-1	4,-1	4,-2	4,1
N=1 (J,M)	2,-2	1,-1	1,-1	2,-2	2,0
Relative Slope (T/THz)	23.9	47.	47.	261.	171.
SQDP*	0.187	2.4×10^{-4}	0.036	1.0×10^{-4}	0.051
Peak Intensity (cm^{-1})**	6.3×10^{-9}	0.8×10^{-11}	1.2×10^{-9}	4×10^{-12}	2×10^{-9}

(2b) ΔM=±1 transitions.

$B_{obs.}$(T)						
$B_{calc.}$(T)	0.4759	0.5206	0.7752	0.8355	0.8411	2.0934
N=3 (J,M) level	2,-1	4,-2	3,-2	4,0	2,-1	4,-1
N=1 (J,M)	2,-2	1,-1	1,-1	2,-1	2,-2	2,0
Relative Slope (T/THz)	32.	33.	57.	55.	103.	181.
SQDP*	0.0458	0.050	0.4×10^{-5}	0.025	0.004	0.037
Peak Intensity (cm^{-1})**	1.6×10^{-9}	1.7×10^{-9}	1.1×10^{-12}	$1.\times10^{-9}$	2×10^{-10}	2×10^{-9}

* See Table 2(1). ** Natural abundance is 0.074%. *** Center of 6-component hfs.

(3) $^{16}O^{18}O$, v=0

(3a) ΔM=0 transitions

$B_{obs.}$(T)	0.6382		1.2458	
$B_{calc.}$(T)	0.63843	1.0999	1.24575	
N=3 (J,M) level	4,-2	3,-1	4,-1	
N=1 (J,M)	2,-2	1,-1	2,-1	
Relative Slope (T/THz)	25.	40.	45.	
SQDP*	0.171	0.0010	0.030	
Peak Intensity (cm^{-1})**	3.1×10^{-8}	2.0×10^{-10}	5.4×10^{-9}	

(3b) ΔM=±1 transitions

$B_{obs.}$(T)	0.83125	0.8875			1.3889
$B_{calc.}$(T)	0.83156	0.88734	0.99727	1.33633	1.38867
N=3 (J,M) level	4,-1	4,-2	3,0	3,-2	4,0
N=1 (J,M)	2,-2	2,-1	1,-1	1,-1	2,-1
Relative Slope (T/THz)	34.	35.	37.	45.	47.
SQDP*	0.044	0.048	0.0007	0.0006	0.0362
Peak Intensity (cm^{-1})**	0.8×10^{-8}	0.9×10^{-8}	1.4×10^{-10}	1.1×10^{-10}	0.7×10^{-8}

*See Table 2(1). ** Natural abundance is 0.408%.

TABLE II—*Continued*

(4) $^{16}O_2$, v=1

(4a) ΔM=0 transitions

$B_{obs.}$(T)		0.18972	0.37955***			
$B_{calc.}$(T)	0.18102	0.18988	0.37988	0.38869	0.90965	1.36694
N=3 (J,M) levels	3,-1	4,-2	4,-1	2,-2	3,0	4,0
N=1 (J,M)	1,-1	2,-2	2,-1	2,-2	1,0	2,0
Relative Slope (T/THz)	68.	23.	47.	99.	249.	164.
SQDP*	1.3×10^{-5}	0.197	0.0415	1.8×10^{-4}	3.0×10^{-4}	1.0×10^{-3}
Peak Intensity (cm^{-1})**	6×10^{-13}	9.4×10^{-9}	2.0×10^{-9}	8.6×10^{-12}	1×10^{-11}	5×10^{-11}

(4b) ΔM=±1 transition

$B_{obs.}$(T)				0.2579	0.2699				0.98194		
$B_{calc.}$(T)	0.15441	0.22789	0.22816	0.25693	0.26889	0.34240	0.65813	0.66743	0.98233	1.03001	2.0010
N=3 (J,M) levels	3,0	3,-2	4,-1	2,-1	4,-2	4,0	3,1	4,1	4,-1	2,-3	3,-1
N=1 (J,M)	1,-1	1,-1	2,-2	2,-2	2,-1	2,-1	1,0	2,0	2,0	1,-2	1,0
Relative Slope (T/THz)	59.	86.	41.	47.	32.	74.	229.	144.	123.	341.	467.
SQDP*	3.1×10^{-6}	3.3×10^{-6}	0.014	0.021	0.051	0.0035	3×10^{-4}	0.0055	0.0548	0.0011	0.0011
Peak Intensity (cm^{-1})**	2×10^{-13}	2×10^{-13}	6.8×10^{-10}	9.9×10^{-10}	2.5×10^{-9}	2×10^{-10}	2×10^{-11}	3×10^{-10}	2.6×10^{-9}	5×10^{-11}	5×10^{-11}

* See Table 2(1)

** Boltzmann factor at 300 K is 5.1×10^{-4}.

*** Partially overlapped with the last hfs component of the $^{16}O^{17}O$ line centers at 0.3711 Tesla.

Because of the spin-axis coupling (the λ term in the Hamiltonian), the N-quantum number, corresponding to the total mechanical angular momentum of the molecular frame, is not a good quantum number. Instead of N we (*11*) can use n to designate each state at zero field. In an external field even this quantum number n (and also N and J) is not a good quantum number. In Table II we designate each state (upper or lower) by a set of two numbers J and M, where M is the magnetic quantum number while J indicates the value of J quantum number when the energy level is extrapolated to the zero field case adiabatically.

The Van Vleck transformation method in which we take a 3×3 matrix for each N state taking into account the effect of other N states by means of the second-order perturbation theory, and then diagonalize this small matrix, produces results which deviate from the experiment by as much as 10 MHz; therefore, this approach is not sufficiently accurate. The deviation is due to the small separation between the $N = 1$ and $N = 3$ triplets of only 430 GHz compared to the triplet spacing, 60 GHz.

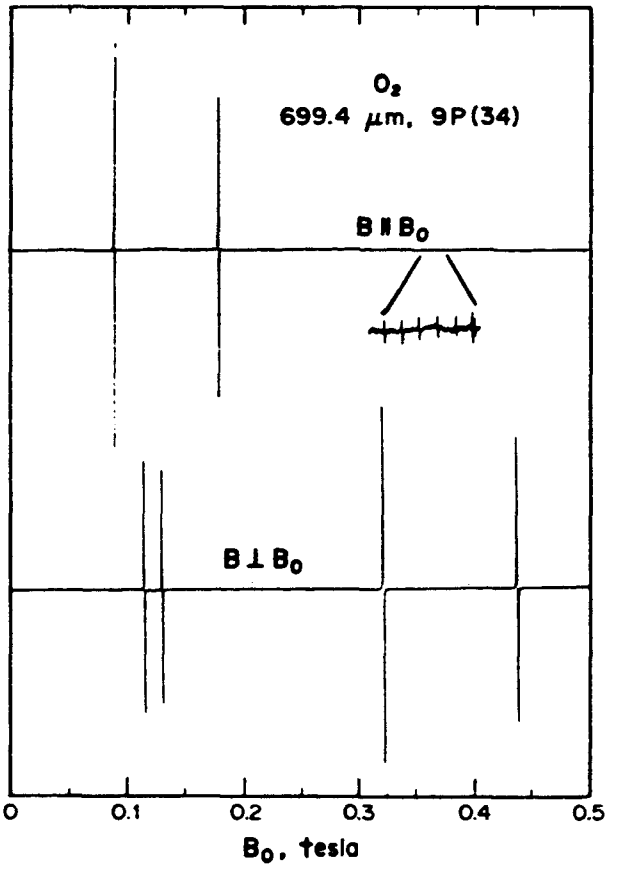

FIG. 2. Typical recorder trace of the 699-μm LMR spectra of oxygen gas. Inset is a section of $B \parallel B_0$ case with the vertical scale amplified 100 times showing hfs of $^{16}O^{17}O$ and one weak line of $^{16}O_2$ in $v = 1$ state.

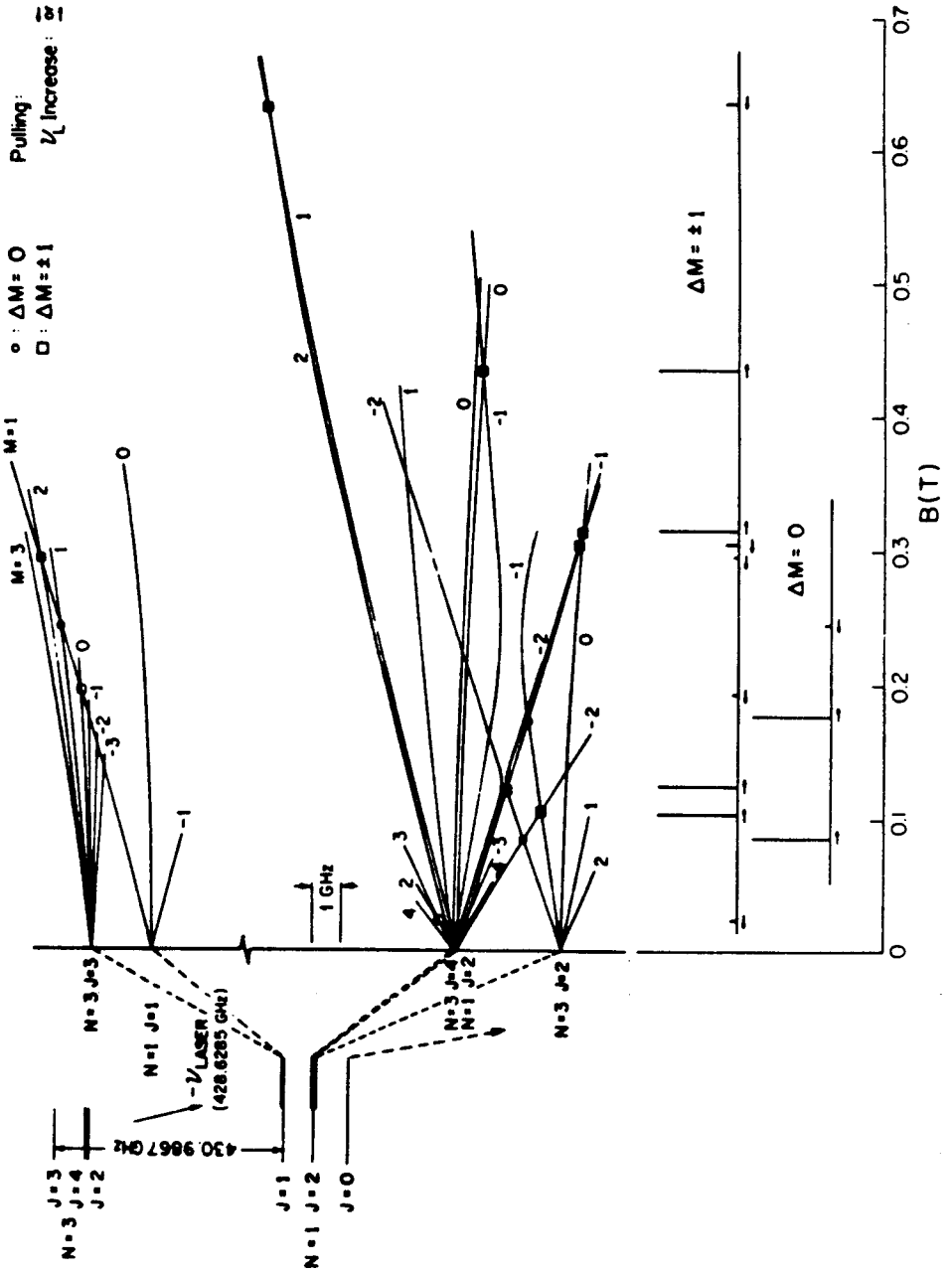
Pulling:
ν_L increase
○ : ΔM = 0
□ : ΔM = ±1
M=1
M=3
N=3 J=3
N=1 J=1
N=3 J=4
N=1 J=2
N=3 J=2
1 GHz
$-\nu_{LASER}$ (428.6285 GHz)
430.9867 GHz
N=3 J=3
J=4
J=2
N=1 J=1
J=2
J=0
ΔM=±1
ΔM=0
B(T)
0
0.1
0.2
0.3
0.4
0.5
0.6
0.7

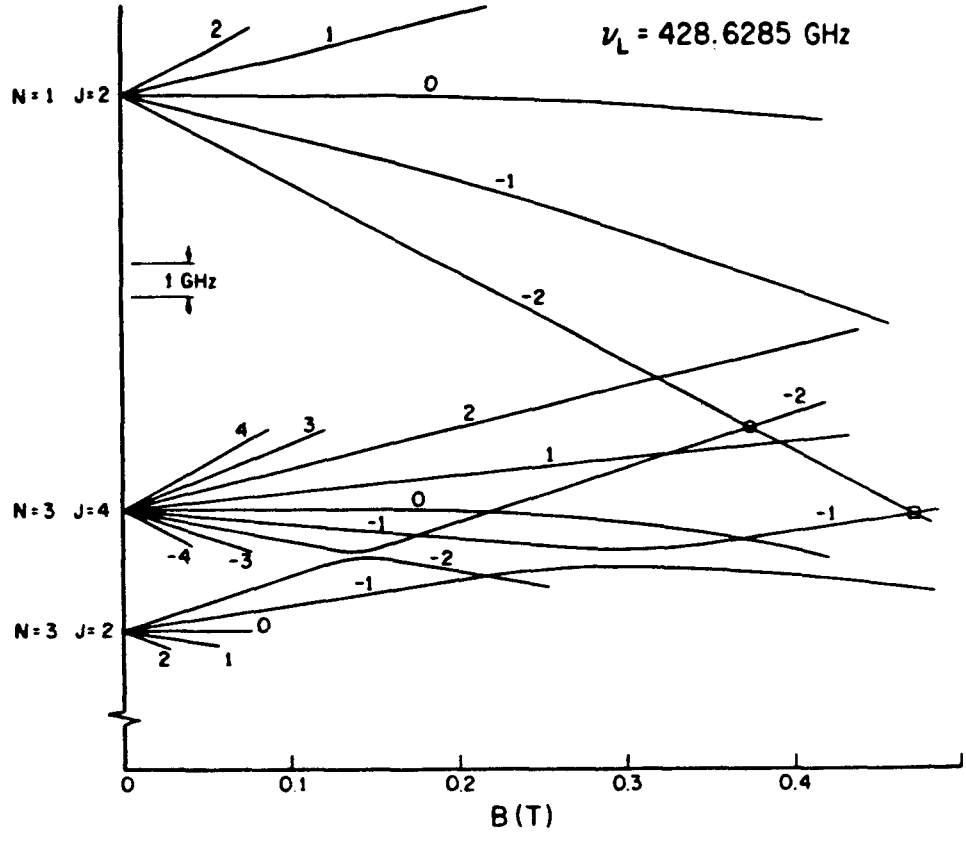

FIG. 4. Levels and laser magnetic resonance for $^{16}O^{17}O$ ($X^3\Sigma_g^-$) $v = 0$.

The relative slope of each resonance line is calculated by diagonalizing the 15 × 15 matrix and is shown in Table II in T/THz (10 G/GHz). The slope indicates how the resonance magnetic field shifts when the resonance frequency is increased by 1 THz. For example, we observed a width of 3.3 mT, on the 0.3034-T line, at about 133 Pa (1 Torr). Therefore, from the slope of −1257 T/THz, we calculate a half-width of 10 kHz/Pa. The half-width of the $N = 3 \leftarrow 1$ line is measured at zero-field (*14*) to be 12.1(12) kHz/Pa in reasonable agreement with our result. However, the width of some of the narrower lines are caused by inhomogeneity of the magnetic field, rather than pressure broadening.

To calculate the peak intensity of each line we first calculate the matrix element of the magnetic moment $2S/\hbar$ in the transition using the eigenvectors obtained in diagonalizing the 15 × 15 matrix. The square of this matrix element, in units of the

FIG. 3. The schematic energy level diagram to illustrate the magnetic resonance at 699 μm. All the $N = 1$ levels are shifted up by the laser frequency so that an appropriate level of $N = 1$ crossed the corresponding one of $N = 3$ at the resonance field of the transition. Levels are for $^{16}O_2$, $v = 0$ (699.4 μm CH_3OH; FIR LMR spectrum).

Bohr magneton, 13.996106 GHz/T, is labeled SQDP and tabulated in Table II for each transition.

If we assume that each line is Lorentzian with width parameter Δ (per Pa), then the absorption coefficient (peak intensity) at the resonance frequency ν (which is the laser frequency in our case) is given by

$$\alpha(\text{peak}) = (\nu\mu_0/\hbar c)(\rho_a - \rho_b)\mu_B^2 \text{SQDP}/\Delta \tag{2}$$

where ρ_a is the number of molecules in the a state per unit volume at 1 Pa and μ_B is the Bohr magneton. This quantity, called the peak intensity, is tabulated in Table II in reciprocal centimeters assuming that Δ is 11.3 kHz/Pa (1.5 MHz/Torr) for all lines. We see that we have observed all stronger lines and that the weakest line we observed in the one at 0.2417 T with the peak intensity of 1.4×10^{-9} cm^{-1}.

Figure 2 shows a typical chart recorder trace and Fig. 3 illustrates the energy levels of the two triplets ($N = 1$ and $N = 3$) as functions of the magnetic field for the $^{16}O_2$, $v = 0$, molecule. The energy of the laser has been added to the $N = 1$ triplet; thus, the crossings corresponding to allowed transitions are the resonances.

$^{16}O^{17}O$ ($X^3\Sigma_g^-$, $v = 0$)

In addition to the lines due to the ordinary oxygen molecule we have observed a few transitions of isotopically substituted oxygen molecules in their natural abundances. We observed the LMR line split into six hyperfine components with spacings of about 1.9 mT at 0.371 T with parallel polarization. This is due to the $^{16}O^{17}O$ molecule in natural abundance (0.074%). The hyperfine structure is due to the ^{17}O nucleus which has spin $I = 5/2$. Microwave transitions of this isotopic molecule was observed by Cazzoli *et al.* (*10*) in enriched sample. They report the value of the molecular parameters which we used with the g factors of the $^{16}O_2$ to calculate LMR spectrum shown in Table II(2). The peak intensity is calculated taking into account the natural abundance.

The peak intensity without hfs is 6.3×10^{-9} cm^{-1}, or 1.1×10^{-9} cm^{-1} for each component, which gives the sensitivity limit of the LMR spectrometer.

If we assume that the nuclear spin is completely decoupled by the external field, but that N and J quantum numbers can be associated to the upper and lower states as ($N = 3$, $J = 2$) and ($N = 1$, $J = 2$), respectively, as seen in Fig. 4, then the spacing is given by $((5/6)b + (c/30))M_I M_J$, where b and c are the hfs coupling constants defined by Frosch and Foley (*15*). From the observed spacing 3.82 mT and the calculated relative slope 0.0239 T/GHz of this line, we see that $|(5b/6) + (c/30)|$ is 79.6 MHz, in very good agreement with Cazzoli *et al.* (*10*) who reported $b = -101.46$ MHz and $c = 139.68$ MHz, which give the spacing constant to be -79.89 MHz.

$^{16}O^{18}O$ ($X^3\Sigma_g^-$, $v = 0$)

Steinbach and Gordy (*9*) observed microwave transitions of the $^{16}O^{18}O$ molecule and obtained the values of the molecular parameters as shown in Table I. We used these values and the g factors of the $^{16}O_2$ molecule, and calculated the LMR spectrum shown in Table II(3). The agreement with five observed lines is quite good.

The natural abundance of this molecule, 0.408%, is multiplied by SQDP in obtaining the peak intensities shown in this table. The weakest line observed at 1.2457 T has the intensity of 5×10^{-9} cm^{-1}.

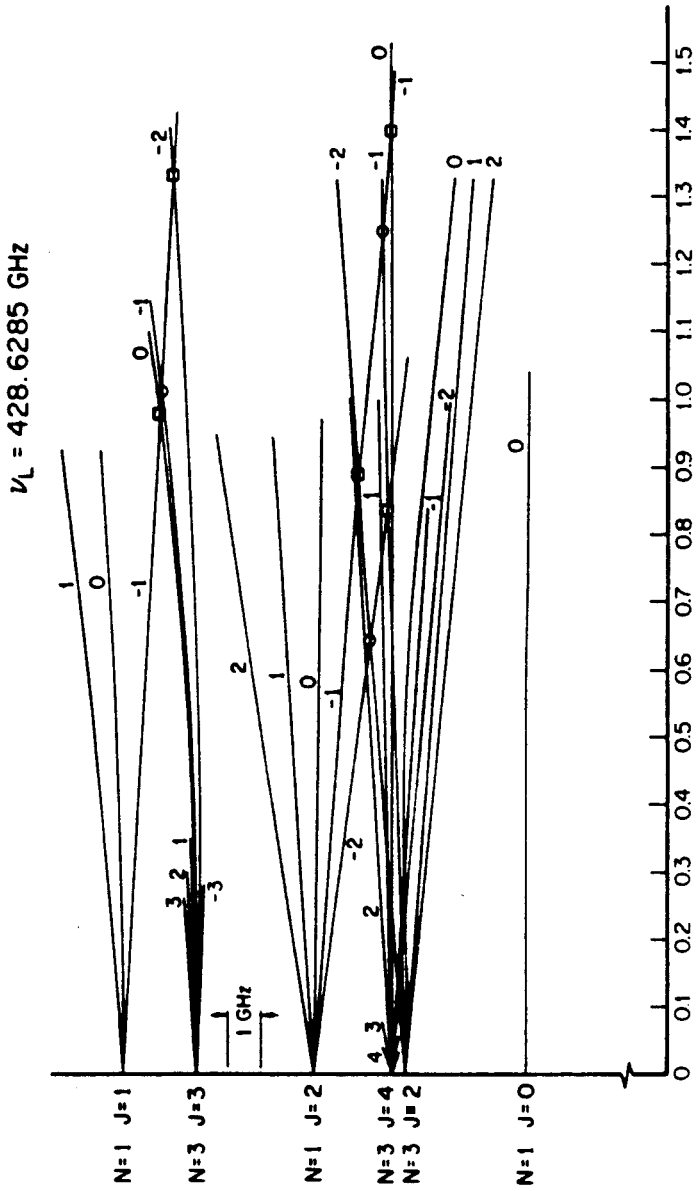

FIG. 5. Levels and laser magnetic resonance for $^{16}O^{18}O$ ($X^3\Sigma_g^-$) $v = 0$.

In Figs. 4 and 5 the Zeeman energy levels of $^{16}O^{17}O$ and $^{16}O^{18}O$, respectively, are illustrated.

$^{16}O_2$ ($X^3\Sigma_g^-$, $v = 1$)

Babcock and Herzberg (*16*) observed vibrationally excited oxygen, and Albritton *et al.* (*17*) reanalyzed their results. Amano and Hirota (*7*) and Endo and Mizushima (*8*) observed some microwave lines due to this species and obtained the values of the molecular parameters. We calculated the LMR spectrum using the last set of values and these values of the g factors given in (*1*). The results are shown in Table II (4).

The relative population of the $v = 1$ level is given by the Boltzmann factor $\exp(-E/kT)$, where $E = 1556.2$ cm^{-1}. The peak intensities shown in Table II(4) are calculated for T = 300 K. It is seen that the line at 0.37964 T is observed within the hfs of $^{16}O^{17}O$ line centered at 0.3711 T, and the intensity of that line is slightly larger than that of each component of hfs. The calculated peak intensity of this line, 2.0×10^{-9} cm^{-1}, is larger than that of each hfs component, 1.1×10^{-9} cm^{-1} in agreement with experiment. On the other hand we did not see a line predicted at 0.22816 T with peak intensity 0.7×10^{-9} cm^{-1}. Therefore the sensitivity limit of this spectrometer is between 1.1 and 0.7 in 10^{-9} cm^{-1}.

The Zeeman energy levels and resonance transitions of this species are shown in Fig. 6.

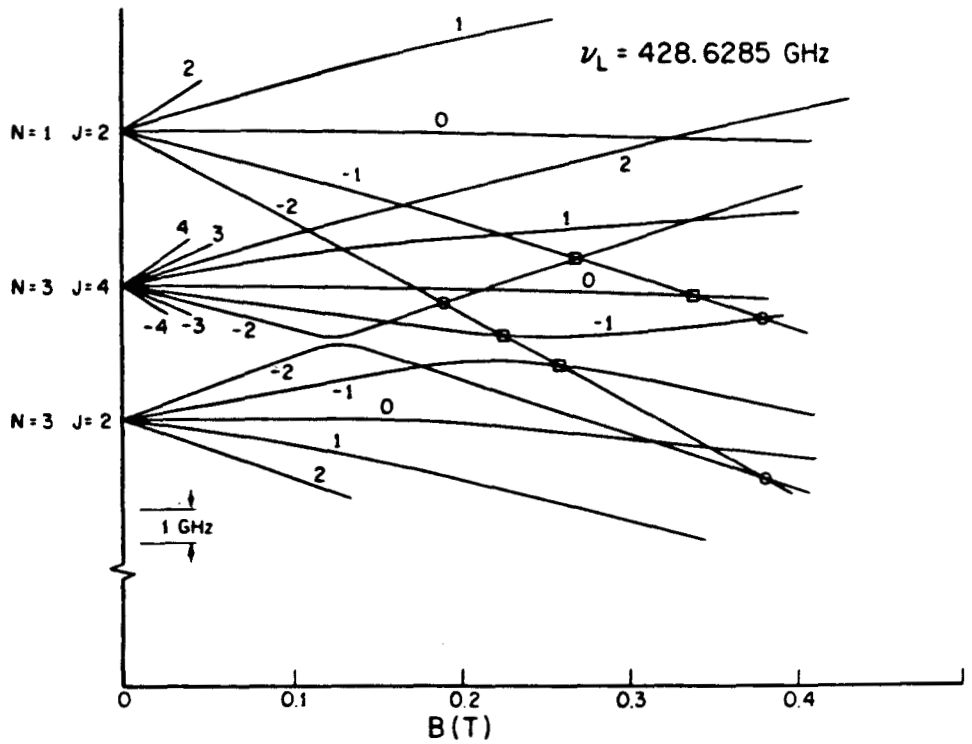

FIG. 6. Levels and laser magnetic resonance for $^{16}O_2$, ($X^3\Sigma_g^-$) $v = 1$.

CONCLUSION

All of the 21 observed LMR transitions are nicely assigned in this analysis. The calculation of the peak intensity has provided us with an estimation of the sensitivity of the spectrometer as between 1.1 and 0.7 in 10^{-9} cm^{-1} at a wavelength of 700 μm with a 1-sec time constant. The spectrometer can also be used to measure pressure broadened linewidths.

ACKNOWLEDGMENT

We thank Dr. R. F. Curl for his reading of this manuscript and his helpful suggestions.

RECEIVED: April 12, 1983

REFERENCES

1. K. M. EVENSON, H. P. BROIDA, J. S. WELLS, R. J. MAHLER, AND M. MIZUSHIMA, *Phys. Rev. Lett.* **21**, 1038–1040 (1968).
2. M. MIZUSHIMA, J. S. WELLS, K. M. EVENSON, AND W. M. WELCH, *Phys. Rev. Lett.* **29**, 831–833 (1972).
3. K. M. EVENSON AND M. MIZUSHIMA, *Phys. Rev. Sect. A* **6**, 2197–2204 (1972).
4. L. TOMUTA, M. MIZUSHIMA, C. J. HOWARD, AND K. M. EVENSON, *Phys. Rev. Sect. A* **12**, 974–979 (1975).
5. J. S. MCKNIGHT AND W. GORDY, *Phys. Rev. Lett.* **21**, 1787–1789 (1968).
6. W. STEINBACH AND W. GORDY, *Phys. Rev. Sect. A* **8**, 1753–1758 (1973).
7. T. AMANO AND E. HIROTA, *J. Mol. Spectrosc.* **53**, 346–363 (1974).
8. Y. ENDO AND M. MIZUSHIMA, *Japan J. Appl. Phys.* **21**, L379–L380 (1982).
9. W. STEINBACH AND W. GORDY, *Phys. Rev. Sect. A* **11**, 729–731 (1975).
10. G. CAZZOLI, C. DEGLI ESPOSTI, P. G. FAVERO, AND G. SEVERI, *Nuovo Cimento B* **62**, 243–255 (1981).
11. M. MIZUSHIMA, "The Theory of Rotating Diatomic Molecules," pp. 265–266, Wiley, New York, 1975.
12. R. W. ZIMMERER AND M. MIZUSHIMA, *Phys. Rev.* **121**, 152–155 (1961); B. G. West and M. Mizushima, *Phys. Rev.* **143**, 31–32 (1966).
13. K. D. BAUER, R. A. KAMPER, AND C. D. LUSTIG, *Proc. R. Soc. (London) Ser. A* **251**, 565–574 (1956).
14. H. M. PICKETT, E. A. COHEN, AND D. E. BRINZA, *Astrophys. J.* **248**, L49–L51 (1981).
15. R. A. FROSCH AND H. M. FOLEY, *Phys. Rev.* **88**, 1337–1349 (1952).
16. H. D. BABCOCK AND L. HERZBERG, *Astrophys. J.* **108**, 167–190 (1948).
17. D. L. ALBRITTON, W. J. HARROP, A. L. SCHMELTKOFF, AND R. N. ZARE, *J. Mol. Spectrosc.* **46**, 103–118 (1973).